Coordinated Dynamic Voltage Support From Inverter-Based Resources

Yifei Guo, *Senior Member, IEEE,* Cong Lei, Bikash C. Pal, *Fellow, IEEE,* Rabih A. Jabr, *Fellow, IEEE* and Haoquan Wang

***Abstract*—This paper presents an optimization approach for coordinated dynamic voltage support (coDVS) using inverter-based resources (IBRs) to enhance network-wide capability of riding through voltage disturbances. Specifically, an optimal coDVS model is developed to alleviate voltage sags in distribution networks. The model is essentially non-convex and hard to solve in general; however, it admits an exact convex semidefinite programming (SDP) relaxation, enabling us to retrieve the globally optimal solution. We prove the equivalence in theory between the current-based and voltage-based formulations of the coDVS problem, even under the SDP relaxation, while justifying that the current-based one is numerically more stable. Furthermore, the approach is extended to address voltage swells and voltage unbalances, unifying the treatment under abnormal voltage conditions. Numerical tests on 33, 69, 95 and 3146-bus distribution networks demonstrate the exactness of the SDP relaxation as well as the numerical issue associated with the voltage-based formulations. Dynamic simulations under typical abnormal voltage conditions further validate the effectiveness of the proposed method.**

***Index Terms*—Dynamic voltage support (DVS), high-voltage ride-through (HVRT), inverter-based resource (IBR), low-voltage ride-through (LVRT), voltage unbalance attenuation (VUA).**

A. Abbreviations

coDVS	Coordinated dynamic voltage support.
HVRT	High-voltage ride-through.
IBR	Inverter-based resource.
LVRT	Low-voltage ride-through.
PCC	Point of common coupling.
PLL	Phase locked-loop.
QCQP	Quadratically-constrained quadratic program.
SDP	Semidefinite programming.
VUA	Voltage unbalance attenuation.

B. Parameters

Y, Z	Network admittance/impedance matrices.
V_s	Slack bus voltage.
$I_i^{\max}$	Current limit of the IBR at bus i.
$P_i^{\max}, P_i^{\min}$	Maximum and minimum active power limits of IBR at bus i.
$\mathcal{N}_0, \mathcal{N}$	Sets of all buses including and excluding the substation bus.
$\mathcal{K}, \mathcal{G}$	Sets of critical buses and IBRs buses.

This work was supported by the Smart Grid-National Science and Technology Major Project under Grant 2025ZD0804300. (*Corresponding author: Yifei Guo*)

Yifei Guo, Cong Lei and Haoquan Wang are with the Key Laboratory of Power System Intelligent Dispatch and Control of Ministry of Education, Shandong University, Jinan 250061, China. (e-mail: yifei.guo@sdu.edu.cn; 202520797@mail.sdu.edu.cn; 202521059@mail.sdu.edu.cn)

Bikash C. Pal is with Electrical and Electronic Engineering Department, Imperial College London, SW7 2AZ London, U.K. (e-mail: b.pal@imperial.ac.uk)

Rabih A. Jabr is with the Department of Electrical and Computer Engineering, American University of Beirut, Beirut 1107 2020, Lebanon (e-mail: rabih.jabr@aub.edu.lb)

C. Variables

$I_i^{\mathrm{d}}, I_i^{\mathrm{q}}$	Positive/negative-sequence active and reactive currents of IBR at bus i.
$V_i, \mathbf{v}$	Complex positive/negative-sequence voltage at bus i; vector of v_i at all buses.
$I_i, \mathbf{i}$	Complex positive/negative-sequence current injection at bus i; vector of I_i at all buses.
X, W	Lifted Hermitian matrices for current and voltage-based SDP relaxations.

D. Notations

$\mathbb{C}, \mathbb{C}^n, \mathbb{R}^n$	Sets of complex numbers, n-dimensional complex vectors and n-dimensional real vectors.
$\mathbb{H}^n$	Set of all $n \times n$ Hermitian matrices.
$\mathrm{Re}\{\cdot\}, \mathrm{Im}\{\cdot\}$	Real/imaginary parts of a complex variable.
$\{\cdot\}^{\mathsf{T}}, \{\cdot\}^{\mathsf{H}}$	Transpose/conjugate transpose operators.
$\mathrm{Tr}\{\cdot\}$	Trace of a matrix
$\mathrm{Rank}\{\cdot\}$	Rank of a matrix.

I. INTRODUCTION

WITH the continuously increased penetration, renewables are now required to provide stability services similar to those of conventional power generation [1], [2]. Specifically, it has reached a consensus that inverter-based resources (IBRs), such as wind and solar PV, must be capable of riding through voltage disturbances (sags, swells, or unbalances) for a certain period of time while providing dynamic voltage support (DVS) to the grid [3].

Within the broad spectrum of control strategies, a prevalent approach is to have IBRs inject positive- or negative-sequence reactive currents in proportion to the severity of voltage disturbances, i.e., the droop-like rules [4]–[8]. These methods are established on the underlying assumption of a strong coupling between reactive power and voltage magnitude; thus, their performance may largely degrade in grids with high R/X ratios. Besides, their heuristic nature may result in suboptimal DVS.

Optimization techniques have recently gained popularity to advance DVS from IBRs in various contexts, e.g., positive-sequence voltage boosting [9], [10] or voltage unbalance attenuation (VUA) [9], [11], [12]. Unlike heuristic strategies, the optimization-based methods can maximize the DVS capability of an IBR while explicitly respecting its physical constraints. Note that these strategies are developed from a standpoint of a single IBR (hereinafter referred to as the "single-IBR" case), focusing on the local voltage performance at the point of common coupling (PCC), where the classical single-machine infinite-bus model is usually adopted. Owing to the simple system structure, certain optimality properties—for example, the results reported in [10]–[12]—can be derived analytically. Nevertheless, such a model inherently falls short in capturing interactions among multiple IBRs or assessing their impact on network-wide voltage performance.

With the large-scale integration of IBRs into power systems, their role has expanded beyond providing DVS solely at their own PCC. They are increasingly expected to contribute to the system-wide stability as stronger voltage support can improve not only voltage stability but also the frequency and synchronization stability [13], thereby mitigating the risk of large-scale cascading failures. Unlocking the coordination potential of IBRs offers an economically efficient and technically feasible pathway to enhancing network-wide DVS performance without requiring significant additional infrastructure. It therefore calls for a systemic re-envisioning of DVS from IBRs, accounting for the interactions and coordination among spatially dispersed IBRs.

A number of studies have investigated the coordination of multiple IBRs for DVS. For instance, systems with parallel-connected IBRs can be simplified to a single-IBR case for analysis, and then the required current is allocated among individual IBRs in proportion to their ratings or electrical proximity to the PCC [14]–[17]. Indeed, the well-established results for a single IBR [9]–[12] trivially apply to parallel-connected multi-IBR configurations only if the common PCC is solely the node of interest [14], [15]; however, for general structured networks or scenarios involving multiple critical buses to be taken care of, optimality is no longer guaranteed [18]. Without relying on the parallel-connection assumption, [19] proposes a multi-agent based distributed scheme for coordinating reactive current injections from IBRs in a microgrid to achieve a better aggregated DVS at the PCC. It is found that while these works have touched on the coordination among IBRs, they still largely treat multiple IBRs as a lumped entity and concentrate primarily on the single PCC voltage, with little attention to broader network-wide voltage performance. Such a simplification may suffice for small-scale networks, but inherently fails to characterize non-uniform voltage profiles prevalent in large-scale networks with considerable electrical distances and high IBR penetration. Notably, this non-uniformity has been linked to avalanche-like cascading trip-offs of IBRs during voltage disturbances [20], underscoring the need for greater attention of systemic behaviors and more sophisticated coordination.

To this end, explicit network-wide DVS optimization has been explored in several recent studies. For example, [21] and [22] develop model predictive control methods to improve the voltage support performance within large-scale wind farms during and after grid faults. The work in [23] proposes an optimization approach for improving the DVS performance of IBRs to address fault-induced delayed voltage recovery caused by induction motors. Besides, a multi-objective optimization model is developed in [24] to reduce network-wide voltage unbalance. Nevertheless, these approaches generally do not guarantee global optimality, either due to approximate modeling assumptions [21], [22] or the use of heuristic solution algorithms [23], [24]. Furthermore, the computational burden associated with such optimization programs remains a critical concern for practical implementation.

So, despite the increasing employment of optimization, the optimality of coordination within multi-IBR networks has yet to be rigorously established. Our previous work [11] gives a glimpse of the optimal coordination among multiple IBRs for VUA from a multi-objective optimization perspective. By relaxing the active power constraints of the IBRs, that study formulates a convex and tractable model, enabling a rigorous analytical derivation of optimality. The optimal solutions derived for the single-IBR case are then generalized and examined in the context of multi-IBR networks. However, a general characterization of optimality remains elusive, particularly when the active power constraints are explicitly considered.

This work revisits the coordinated dynamic voltage support (coDVS) problem in distribution networks with multiple IBRs through the lens of optimization. In contrast to a single-IBR case or simplified multi-IBR settings with relaxed active power constraints, an analytical characterization of optimality becomes considerably more challenging due to the increased problem size and inherent nonconvexity. Hence, this paper resorts to numerical optimization techniques. Specifically, the contributions of this paper are summarized as follows.

1) Exemplified in the context of low-voltage-ride-through (LVRT), we develop a *(positive-)sequence voltage maximization* model with nodal current injections as the decision variables. Given that the cost function and active power constraints are not convex, the model is inherently a nonconvex quadratically-constrained quadratic program (QCQP) and thus hard to solve in general. So, we convexify it by a semidefinite programming (SDP) relaxation that is efficiently solvable. Interestingly, such relaxation is shown to be exact for all the test cases, from which the globally optimal solution (to the original QCQP) can be recovered.
2) Inspired by the well-established optimal power flow models [25], we propose an alternative voltage-based formulation of coDVS while giving its SDP relaxation. We prove the theoretical equivalence between the current-based and voltage-based formulations, both before and after the SDP relaxation, and show that the latter is inherently prone to numerical issues when solved by practical SDP solvers.
3) We extend the approach to address voltage swells or unbalances and to accommodate nondispatchable IBRs with fixed power setpoints. Crucially, the proposed SDP relaxation-based solution approach remains applicable to these extended scenarios.

Notably, the proposed coDVS solution can be implemented directly as a centralized optimal control strategy. Moreover, it provides a theoretical foundation for the development of decentralized (near-)optimal control schemes, particularly when integrated with advanced data-driven techniques [26], [27], while also serving as a benchmark for evaluating other alternative methods.

The rest of this paper is organized as follows. Section II presents the coDVS problem formulation in the context of positive-sequence voltage maximization. Section III develops an SDP relaxation-based solution approach for the resulting nonconvex QCQP problem. Section IV introduces the alternative nodal voltages-based formulation along with its SDP relaxation, proves the equivalence between current-based and voltage-based formulations, and discusses several computa-

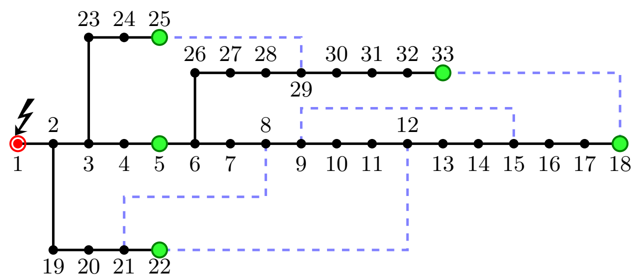

Fig. 1. IEEE 33-bus distribution network with five IBRs (at the green nodes).

tional issues. The approach is extended in Section V to address voltage swells/unbalances and non-dispatch IBRs. Section VI and VII present numerical validation and dynamic simulation results, respectively. Finally, section VIII concludes the paper.

II. Problem Formulation

We illustrate the proposed method using the LVRT scenario as an example, with the primary goal of boosting positive-sequence voltage. To allow for a decoupled sequence network analysis, the network is assumed to be structurally symmetrical; that is, each line segment is three-phase with (nearly) symmetrical line parameters, or the network is single-phase. For notational simplicity, the physical quantities, including admittance (Y), impedance (Z), voltage (V_i), and current (I_i), refer to their positive-sequence components throughout Section II and will be slightly abused in Section V to represent the negative-sequence counterparts where appropriate.

A. System Models

Consider a distribution network with a set of buses $\mathcal{N}_0 := \{1, 2, \ldots, n\}$ where the substation bus (slack bus) is indexed by '1' and let $\mathcal{N} := \mathcal{N}_0 \backslash \{1\}$; an illustrative example is shown in Fig. 1. Let $V_i \in \mathbb{C}$ and $I_i \in \mathbb{C}$ be the complex voltage and current injection phasors at bus i, respectively. Define $\mathbf{i} := [I_1, I_2, \ldots, I_n]^\mathsf{T}$ and $\mathbf{v} := [V_1, V_2, \ldots, V_n]^\mathsf{T}$, which are related by the Kirchhoff's current law

$$\mathbf{i} = Y\mathbf{v} \tag{1}$$

where $Y \in \mathbb{C}^{n\times n}$ is the network admittance matrix accounting for all distribution line segments, shunt elements, and constant-impedance loads modeled as shunt admittances. Assume Y is nonsingular, which usually holds true in practice under some mild conditions [28]. Let $Z := Y^{-1}$.

Without loss of generality, the IBRs in this work are assumed to operate in grid-following mode and employ the typical cascading control [29], [30]. In presence of considerable voltage sags, the outer-loop control opts out, and the IBR's current is instead governed by a dedicated DVS controller. So, IBRs behave as an independent current source subject to the current and power constraints:

$$|I_i|^2 \le (I_i^{\max})^2, \qquad i \in \mathcal{N} \tag{2}$$

$$P_i^{\min} \le \mathrm{Re}\{V_i \cdot I_i^\mathsf{H}\} \le P_i^{\max}, \qquad i \in \mathcal{N} \tag{3}$$

where for pure load buses, $I_i^{\max}$, $P_i^{\max}$, and $P_i^{\min}$ are all equal to 0 in per unit.

It is worth noting that although we base our approach on the assumption of grid-following operation in this paper, it is in fact technology-neutral. The formulation naturally applies to the systems incorporating grid-forming IBRs as well, as they are likewise subject to the similar current and active power constraints as defined in (2) and (3). The only distinction lies in how the optimal solution is implemented within the respective IBR control systems.[1]

B. Optimal Current Injection Model for Coordinated DVS

During voltage sags, the coDVS seeks to optimize the holistic voltage support performance across a set of predefined critical buses, e.g., the ones with critical loads or generators by coordinating the current injections of IBRs, subject to power flow constraint (1), IBRs' current constraints (2), and IBRs' active power injection constraints (3). It is formulated as a *sequence voltage maximization* model:

$$\begin{aligned}
\max_{\mathbf{v},\mathbf{i}\in\mathbb{C}^n} \quad & \mathbf{v}^\mathsf{H} C \mathbf{v} && \text{(4a)}\\
\text{subject to} \quad & \mathbf{i} = Y\mathbf{v} && \text{(4b)}\\
& |I_i|^2 \le (I_i^{\max})^2, \qquad i \in \mathcal{N} && \text{(4c)}\\
& \mathrm{Re}\{V_i \cdot I_i^\mathsf{H}\} \le P_i^{\max}, \quad i \in \mathcal{N} && \text{(4d)}\\
& \mathrm{Re}\{V_i \cdot I_i^\mathsf{H}\} \ge P_i^{\min}, \quad i \in \mathcal{N} && \text{(4e)}\\
& |V_1|^2 = V_s^2 && \text{(4f)}
\end{aligned}$$

where $C := \mathrm{diag}(c_1, c_2, \ldots, c_n)$ is the weighting matrix, and $c_i \ge 0$ quantifies the importance of buses. V_s is the slack bus voltage magnitude, which collectively represents the voltage disturbances originated from the external system. It is a fixed value in the optimization program.

Eliminating the complex voltages using (1), the problem can be cast as a complex-valued QCQP:

$$\begin{aligned}
\textbf{c-QCQP}: \min_{\mathbf{i}\in\mathbb{C}^n} \quad & -\mathbf{i}^\mathsf{H} M^\mathrm{v} \mathbf{i} && \text{(5a)}\\
\text{subject to} \quad & \mathbf{i}^\mathsf{H} M_i^\mathrm{c} \mathbf{i} \le (I_i^{\max})^2, \ i \in \mathcal{N} && \text{(5b)}\\
& \mathbf{i}^\mathsf{H} M_i^\mathrm{p} \mathbf{i} \le P_i^{\max}, \ i \in \mathcal{N} && \text{(5c)}\\
& \mathbf{i}^\mathsf{H} M_i^\mathrm{p} \mathbf{i} \ge P_i^{\min}, \ i \in \mathcal{N} && \text{(5d)}\\
& \mathbf{i}^\mathsf{H} M_s^\mathrm{v} \mathbf{i} = V_s^2 && \text{(5e)}
\end{aligned}$$

where only the current injections of IBRs serve as the decision variables. The parameter matrices are given by

$$\begin{aligned}
M^\mathrm{v} &= Z^\mathsf{H} C Z\\
M_i^\mathrm{c} &= \mathbf{e}_i \mathbf{e}_i^\mathsf{T}\\
M_i^\mathrm{p} &= \frac{Z^\mathsf{H}\mathbf{e}_i\mathbf{e}_i^\mathsf{T} + \mathbf{e}_i\mathbf{e}_i^\mathsf{T} Z}{2}\\
M_s^\mathrm{v} &= Z^\mathsf{H}\mathbf{e}_1\mathbf{e}_1^\mathsf{T} Z
\end{aligned}$$

where $\mathbf{e}_1, \mathbf{e}_2, \ldots, \mathbf{e}_n$ denote the standard basis vectors in $\mathbb{R}^n$.

[1]Specifically, for grid-forming IBRs entering current saturation during disturbances, the optimal current setpoints can be accurately tracked by employing a dedicated feedback loop that dynamically aligns the local dq-frame with the instantaneous voltage phase angle.

III. Solution via Semidefinite Relaxation

Given that $M^{\mathrm{v}} \succeq 0$ and M_i^{p} is indefinite, the problem (5) is nonconvex and therefore hard to solve generally. Hence, in this section, we propose solving its convex relaxation, from which the globally optimal solution (optimal solution hereinafter for short) can be recovered if the relaxation is exact.

First, lift the vector $\mathbf{i} \in \mathbb{C}^n$ to a Hermitian matrix $X = \mathbf{i}\mathbf{i}^{\mathsf{H}}$, which is equivalent to

$$X \succeq 0,\ \operatorname{rank}\{X\} = 1.$$

Then, replacing $\mathbf{i}$ by X and relaxing the nonconvex rank constraint, one can obtain an SDP relaxation (also known as the Shor relaxation) of (5),

$$\begin{aligned}
\textbf{c-SDP}: \min_{X \in \mathbb{H}^n} \quad & \operatorname{Tr}\{-M^{\mathrm{v}} X\} && \text{(6a)}\\
\text{subject to} \quad & \operatorname{Tr}\{M_i^{\mathrm{c}} X\} \le (I_i^{\max})^2,\ i \in \mathcal{N} && \text{(6b)}\\
& \operatorname{Tr}\{M_i^{\mathrm{p}} X\} \le P_i^{\max},\ i \in \mathcal{N} && \text{(6c)}\\
& \operatorname{Tr}\{M_i^{\mathrm{p}} X\} \ge P_i^{\min},\ i \in \mathcal{N} && \text{(6d)}\\
& \operatorname{Tr}\{M_s^{\mathrm{v}} X\} = V_s^2 && \text{(6e)}\\
& X \succeq 0. && \text{(6f)}
\end{aligned}$$

This program can be solved using many off-the-shelf numerical SDP solvers.

Clearly, the optimal objective value of the c-SDP provides a lower bound on that of the c-QCQP. It is well known that for nonconvex QCQP problems, such bound is *not* tight in general. However, as verified in the test cases of this work, the SDP relaxation is *exact* for this problem, which enables a successful recovery of the optimal solution to the c-QCQP.

If the c-SDP returns a rank-one solution $X^\star$, a globally optimal solution to the c-QCQP can then be recovered as follows:

$$\mathbf{i}^\star = \sqrt{\lambda}\mathbf{x}^\star \tag{7}$$

where λ is the unique non-zero eigenvalue of $X^\star$, and $\mathbf{x}^\star$ is the associated unit-length eigenvector.

IV. Voltage-Based Formulation and Equivalence

Many well-established optimal power flow models usually adopt nodal voltages, instead of current injections, as the decision variables[2]; see [25] for a survey. Motivated by this convention, we here present an alternative formulation based on complex nodal voltages and also discuss its relation with the current-based formulation.

A. Voltage-Based Formulation

The voltage-based formulation can be derived by eliminating the complex currents, which is as follows:

$$\begin{aligned}
\textbf{v-QCQP}: \min_{\mathbf{v} \in \mathbb{C}^n} \quad & -\mathbf{v}^{\mathsf{H}} C \mathbf{v} && \text{(8a)}\\
\text{subject to} \quad & \mathbf{v}^{\mathsf{H}} H_i^{\mathrm{c}} \mathbf{v} \le (I_i^{\max})^2,\ i \in \mathcal{N} && \text{(8b)}\\
& \mathbf{v}^{\mathsf{H}} H_i^{\mathrm{p}} \mathbf{v} \le P_i^{\max},\ i \in \mathcal{N} && \text{(8c)}\\
& \mathbf{v}^{\mathsf{H}} H_i^{\mathrm{p}} \mathbf{v} \ge P_i^{\min},\ i \in \mathcal{N} && \text{(8d)}\\
& \mathbf{v}^{\mathsf{H}} H_s^{\mathrm{v}} \mathbf{v} = V_s^2 && \text{(8e)}
\end{aligned}$$

[2]There may be several reasons for this preference. One notable advantage is computational efficiency: using voltages as decision variables preserves the sparsity structure induced by the admittance matrix, thereby facilitating faster and more efficient numerical computations.

where

$$\begin{aligned}
H_i^{\mathrm{c}} &= Y^{\mathsf{H}} \mathbf{e}_i \mathbf{e}_i^{\mathsf{T}} Y\\
H_i^{\mathrm{p}} &= \frac{Y^{\mathsf{H}} \mathbf{e}_i \mathbf{e}_i^{\mathsf{T}} + \mathbf{e}_i \mathbf{e}_i^{\mathsf{T}} Y}{2}\\
H_s^{\mathrm{v}} &= \mathbf{e}_1 \mathbf{e}_1^{\mathsf{T}}.
\end{aligned}$$

Similarly, lifting the vector $\mathbf{v} \in \mathbb{C}^n$ to a Hermitian matrix $W \in \mathbb{H}^n$, i.e.,

$$W = \mathbf{v}\mathbf{v}^{\mathsf{H}} \iff W \succeq 0,\ \operatorname{rank}\{W\} = 1$$

and relaxing the rank constraint, its SDP relaxation reads as

$$\begin{aligned}
\textbf{v-SDP}: \min_{W \in \mathbb{H}^n} \quad & \operatorname{Tr}\{-CW\} && \text{(9a)}\\
\text{subject to} \quad & \operatorname{Tr}\{H_i^{\mathrm{c}} W\} \le (I_i^{\max})^2,\ i \in \mathcal{N} && \text{(9b)}\\
& \operatorname{Tr}\{H_i^{\mathrm{p}} W\} \le P_i^{\max},\ i \in \mathcal{N} && \text{(9c)}\\
& \operatorname{Tr}\{H_i^{\mathrm{p}} W\} \ge P_i^{\min},\ i \in \mathcal{N} && \text{(9d)}\\
& \operatorname{Tr}\{H_s^{\mathrm{v}} W\} = V_s^2, && \text{(9e)}\\
& W \succeq 0. && \text{(9f)}
\end{aligned}$$

B. Equivalence

With these two pairs of formulations established, we now present their underlying relationships. The main results are summarized in Theorems 1 and 2.

Theorem 1 (Equivalence Between v-QCQP and c-QCQP):v-QCQP and c-QCQP are equivalent in the sense that (i) there exists a bijection between their sets of optimal solutions, and (ii) they yield the same optimal objective value.

Proof: First of all, since the objective function is continuous, and the constraint set is closed and bounded in both the c-QCQP and v-QCQP, the existence of an optimal solution is guaranteed by the Weierstrass Theorem [31].

Then, let $\mathbb{I}$ and $\mathbb{V}$ denote the feasible solution sets of c-QCQP and v-QCQP, respectively

$$\mathbb{I} := \left\{\mathbf{i} \in \mathbb{C}^n \middle| \mathbf{i} \text{ satisfies } (5\text{b}) - (5\text{e})\right\},$$
$$\mathbb{V} := \left\{\mathbf{v} \in \mathbb{C}^n \middle| \mathbf{v} \text{ satisfies } (8\text{b}) - (8\text{e})\right\}$$

and $\mathbb{I}^\star \subseteq \mathbb{I}$ and $\mathbb{V}^\star \subseteq \mathbb{V}$ denote their optimal solution sets.

For every optimal solution to the v-QCQP, $\mathbf{v}^\star \in \mathbb{V}^\star$, let $\mathbf{i}^* := Y\mathbf{v}^\star$. Now, we show that $\mathbf{i}^*$ is exactly an optimal solution to the c-QCQP with the same objective value.

Since (8b)–(8e) are satisfied at $\mathbf{v}^\star$, it is straightforward to check that (5b)–(5e) hold at $\mathbf{i}^*$, i.e., $\mathbf{i}^* \in \mathbb{I}$, and we have

$$\mathbf{i}^{*\mathsf{H}} M^{\mathrm{v}} \mathbf{i}^* = (Y\mathbf{v}^\star)^{\mathsf{H}} M^{\mathrm{v}} (Y\mathbf{v}^\star) = \mathbf{v}^{\star\mathsf{H}} C \mathbf{v}^\star.$$

So, $\mathbf{i}^*$ is a feasible solution to the c-QCQP, preserving the objective value. The remaining is to show it is optimal.

Suppose by contradiction that $\mathbf{i}^* \notin \mathbb{I}^\star$. Then, there exists a solution $\hat{\mathbf{i}} \in \mathbb{I}^\star$, such that

$$\hat{\mathbf{i}}^{\mathsf{H}} M^{\mathrm{v}} \hat{\mathbf{i}} > \mathbf{i}^{*\mathsf{H}} M^{\mathrm{v}} \mathbf{i}^*.$$

Let $\hat{\mathbf{v}} = Z\hat{\mathbf{i}}$. One can easily check that $\hat{\mathbf{v}} \in \mathbb{V}$ and

$$\hat{\mathbf{v}}^{\mathsf{H}} C \hat{\mathbf{v}} = (Z\hat{\mathbf{i}})^{\mathsf{H}} C (Z\hat{\mathbf{i}}) = \hat{\mathbf{i}}^{\mathsf{H}} M^{\mathrm{v}} \hat{\mathbf{i}} > \mathbf{i}^{*\mathsf{H}} M^{\mathrm{v}} \mathbf{i}^* = \mathbf{v}^{\star\mathsf{H}} C \mathbf{v}^\star.$$

which contradicts that $\mathbf{v}^\star \in \mathbb{V}^\star$.

Conversely, one can also show that for every optimal solution to the c-QCQP, $\mathbf{i}^\star \in \mathbb{I}^\star$, $Z\mathbf{i}^\star$ is an optimal solution to the v-QCQP with the same objective value.

Therefore, there exists a bijection ($\mathbf{i}^\star = Y\mathbf{v}^\star$ and $\mathbf{v}^\star = Z\mathbf{i}^\star$) between $\mathbb{I}^\star$ and $\mathbb{V}^\star$, which preserves the objective value. ■

With this in place, an immediate question is whether such equivalence still holds under the SDP relaxation, which is partially addressed by the following theorem.

Theorem 2 (Equivalence Under SDP Relaxation): The v-SDP is exact if and only if the c-SDP is exact.

To derive the equivalence under relaxation, it is crucial to identify the appropriate mappings like (1) between the feasible sets of the c-SDP ($\mathbb{X}$) and v-SDP ($\mathbb{W}$) where

$$\mathbb{X} := \Big\{X \in \mathbb{H}^n \big| X \text{ satisfies } (6\text{b}) - (6\text{f})\Big\},$$
$$\mathbb{W} := \Big\{W \in \mathbb{H}^n \big| W \text{ satisfies } (9\text{b}) - (9\text{f})\Big\}.$$

The following Lemmas construct such mappings and illustrate some associated properties.

Lemma 1 (A Bijective Mapping Between): The linear mapping $f : \mathbb{X} \mapsto \mathbb{W}$ defined by

$$f(X) := ZXZ^{\mathsf{H}}. \tag{10}$$

is bijective, and its inverse $g : \mathbb{W} \mapsto \mathbb{X}$ is given by

$$g(W) := YWY^{\mathsf{H}}. \tag{11}$$

Lemma 2 (Objective Value-Preserving): The mapping $f : \mathbb{X} \mapsto \mathbb{W}$ and its inverse $g : \mathbb{W} \mapsto \mathbb{X}$ are *objective value-preserving*, i.e.,

$$\mathrm{Tr}\{-Cf(X)\} = \mathrm{Tr}\{-M^{\mathrm{v}}X\}, \quad X \in \mathbb{X}$$
$$\mathrm{Tr}\{-M^{\mathrm{v}}g(W)\} = \mathrm{Tr}\{-CW\}, \quad W \in \mathbb{W}.$$

Lemma 3 (Rank-Preserving): The mapping $f : \mathbb{X} \mapsto \mathbb{W}$ and its inverse $g : \mathbb{W} \mapsto \mathbb{X}$ are *rank-preserving*, i.e.,

$$\mathrm{rank}\{f(X)\} = \mathrm{rank}\{X\}, \quad X \in \mathbb{X}$$
$$\mathrm{rank}\{g(W)\} = \mathrm{rank}\{W\}, \quad W \in \mathbb{W}.$$

The proof of Lemma 1 is provided in the Appendix. Lemma 2 follows immediately from the cyclic property of trace operator. Lemma 3 is valid due to the nonsingularity of Y and Z, which ensures that any rank-one solution to the c-SDP (or v-SDP) remains rank-one under the mapping f (or g).

Proof of Theorem 2:

Part 1) c-SDP ⇒ v-SDP: Let $X^\star \in \mathbb{X}$ be a rank-one solution to c-SDP. Consequently, the optimal objective values satisfy

$$O^\star_{\mathrm{cQCQP}} = O^\star_{\mathrm{cSDP}}.$$

It is then obtained from Lemmas 1 and 2 that

$$\mathrm{Tr}\{-CW\} = \mathrm{Tr}\{-M^{\mathrm{v}}g(W)\} \geq \mathrm{Tr}\{-M^{\mathrm{v}}X^\star\}, \;\; W \in \mathbb{W}$$

with the second equality attained if $W = f(X^\star) \in \mathbb{W}$.

From Lemma 3, $\mathrm{rank}\{f(X^\star)\} = \mathrm{rank}\{X^\star\} = 1$.

Then, combining with Theorem 1, one can obtain that

$$O^\star_{\mathrm{vQCQP}} = O^\star_{\mathrm{cQCQP}} = O^\star_{\mathrm{cSDP}} = \mathrm{Tr}\{-Cf(X^\star)\}.$$

Therefore, $f(X^\star) \in \mathbb{W}$ is a rank-one solution to the v-SDP, which implies the v-SDP is exact as well. This completes the proof of Part 1).

Part 2) v-SDP ⇒ c-SDP: Let $W^\star \in \mathbb{W}$ be a rank-one solution to v-SDP. It then follows from Lemmas 1 and 2 that

$$\mathrm{Tr}\{-M^{\mathrm{v}}X\} = \mathrm{Tr}\{-Cf(X)\} \geq \mathrm{Tr}\{-CW^\star\}, \quad X \in \mathbb{X}$$

and the second equality is attained if $X = g(W^\star) \in \mathbb{X}$.

From Lemma 3, $\mathrm{rank}\{g(W^\star)\} = \mathrm{rank}\{W^\star\} = 1$.

Then, combining with Theorem 1, one can obtain that

$$O^\star_{\mathrm{cQCQP}} = O^\star_{\mathrm{vQCQP}} = O^\star_{\mathrm{vSDP}} = \mathrm{Tr}\{-M^{\mathrm{v}}g(W^\star)\}$$

Therefore, $g(W^\star) \in \mathbb{X}$ is a rank-one solution to the c-SDP, which implies that the c-SDP is exact. ■

C. Computational Issues

1) Numerical Stability: Theorems 1 and 2 establish the theoretical equivalence between the current-based and voltage-based formulations, even under the relaxation. In other words, either formulation can be solved without compromising optimality. However, it is worth noting that the v-SDP may suffer from numerical problems, due to the ill-conditioned nature of the model. This issue is primarily attributable to the current constraint (9b). Specifically, the small impedance of short distribution lines (in per unit) may lead to nonzero entries with a large absolute value in the admittance matrix Y. Recall that $H^{\mathrm{c}}_i = Y^{\mathsf{H}}\mathbf{e}_i\mathbf{e}_i^{\mathsf{T}}Y$, of which the entries in absolute value would be $|Y^{\mathsf{H}}_{ij}Y_{ik}|$. This can lead to a large spread in the order of magnitudes among model coefficients, which poses numerical challenges during computation. In contrast, the c-SDP formulation exhibits greater numerical stability, as the entries in Z tend to vary within a much more moderate range.

2) Complexity Reduction: The current-based formulation allows for a reduction in problem size. By retaining only the current injection variables associated with the slack bus and IBR buses, the reduced model can be partitioned as

$$\begin{bmatrix} V_1 \\ \mathbf{v}_{\mathcal{K}} \end{bmatrix} = \begin{bmatrix} Z_{11} & Z_{1\mathcal{G}} \\ Z_{\mathcal{K}1} & Z_{\mathcal{K}\mathcal{G}} \end{bmatrix} \begin{bmatrix} I_1 \\ \mathbf{i}_{\mathcal{G}} \end{bmatrix} \tag{12}$$

where $\mathcal{K} \subseteq \mathcal{N}$ is the set of critical buses to be optimized ($c_i > 0$ for $i \in \mathcal{K}$, and $c_i = 0$ otherwise); $\mathcal{G} \subseteq \mathcal{N}$ is the set of IBR buses; $\mathbf{v}_{\mathcal{K}}$ denotes the vector collecting all critical bus voltages; $\mathbf{i}_{\mathcal{G}}$ denotes the vector collecting all IBRs' current injections; Z_{11}, $Z_{1\mathcal{G}}$, $Z_{\mathcal{K}1}$, and $Z_{\mathcal{K}\mathcal{G}}$ represent the corresponding submatrices of Z. Given that $|\mathcal{G}| \ll |\mathcal{N}|$ in many practical cases, the reduced formulations are computationally more tractable, particularly in the context of SDP relaxation.

3) Realification: Most numerical solvers only handle real-valued data. Thus, when a complex-valued SDP is formulated, the solvers internally or externally convert it into a real-valued equivalent form before calling the core numerical routines.

V. Extensions

A. Addressing Voltage Swell and Voltage Unbalance

To address voltage swell (or unbalance), positive-sequence (or negative-sequence) voltage should be reduced, which uniformly relies on a *sequence voltage minimization* model:

$$\min_{\mathbf{v},\mathbf{i} \in \mathbb{C}^n} \quad \mathbf{v}^{\mathsf{H}}C\mathbf{v} \quad \text{subject to} \quad (4\text{b}) - (4\text{f}). \tag{13}$$

Similarly, it can also be recast into a (nonconvex) QCQP with either voltages or currents being the decision variables, to which the SDP relaxation technique is still applicable. Note that in the context of voltage unbalance mitigation scenarios, the quantities (for example, $\mathbf{v}$, $\mathbf{i}$, Y and Z) in (13) refer to the negative-sequence ones wherever appropriate.

In spite of the change in the objective function, the equivalence between the current-based and voltage-based formulations still holds, even under the SDP relaxation. The proof is analogous to the ones associated with the *sequence voltage maximization* problem and is therefore omitted for brevity.

B. Accounting for Non-dispatchable IBRs

The proposed method is inherently capable of incorporating non-dispatchable IBRs in a unified manner. During grid disturbances, some IBRs may remain in their pre-fault operating modes (e.g., maintaining MPPT) rather than actively participating in the coDVS. The impact of these units on network voltages can be seamlessly integrated into the optimization by enforcing fixed power setpoints. For an IBR at bus i that maintains its pre-fault power references $P_i^{\rm ref}$ and $Q_i^{\rm ref}$, the active and reactive power constraints are given as:

$$\mathbf{i}^{\mathsf{H}} M_i^{\rm p} \mathbf{i} = P_i^{\rm ref}, \quad \mathbf{i}^{\mathsf{H}} M_i^{\rm q} \mathbf{i} = Q_i^{\rm ref} \tag{14}$$

where $M_i^{\rm q} = (\mathbf{e}_i \mathbf{e}_i^{\mathsf{T}} Z - Z^{\mathsf{H}} \mathbf{e}_i \mathbf{e}_i^{\mathsf{T}})/2\mathrm{j}$. In this way, the structural integrity of the optimization model [e.g. (5)] is preserved.

Moreover, as will be demonstrated shortly, the SDP relaxation under the above extensions remains exact. This enables a unified treatment of coDVS of IBRs across various contexts.

VI. Numerical Validation

We first numerically test the proposed optimal coDVS on the IEEE 33-bus [32], IEEE 69-bus [33], UKGDS 95-bus test feeders [34], and a real-world 3146-bus system [35]. A few test scenarios are designed to examine its effectiveness under various abnormal voltage conditions, including voltage sags, swells, and unbalances. The detailed configurations of the test systems are described as follows:

- In the IEEE 33-bus, IEEE 69-bus, and UKGDS 95-bus test feeders, five, seven, and eight IBRs are dispersedly installed, respectively. Each IBR has a power rating of 1 MW and an inverter overcurrent capability of 150% of the rated value.
- In the 3146-bus system, we randomly select 50 buses for IBR deployment. The power ratings of IBRs are randomly assigned within the range of $0.1 \sim 1$ MW, featuring an overcurrent capability of 200% of the rated value.

The SDP problems are solved using SeDuMi [36] unless otherwise specified, invoked through the MATLAB toolbox YALMIP [37].

A. Optimality: Exactness of SDP Relaxation

Tables I – IV summarize the numerical results on the test feeders, where different combinations of voltage disturbances and power availability levels of IBRs are considered. Both c-SDP and v-SDP of the test feeders are solved and compared. Without loss of generality, let $c_i = 1$ for all $i \in \mathcal{N}$, i.e., $\mathcal{K} = \mathcal{N}$. The symbols within the tables are interpreted below:

- The 'LVRT', 'HVRT', and 'VUA' stand for the low-voltage-ride-through under voltage sags, high-voltage-ride-through under voltage swells, and voltage unbalance attenuation, respectively.

TABLE I
Numerical Results of IEEE 33-Bus Test Feeder

Case	V_s	$\frac{P_i^{\max}}{S_i}$	$\frac{P_i^{\min}}{S_i}$	$\frac{\lambda_2\{X^\star\}}{\lambda_1\{X^\star\}}$	$\frac{\lambda_2\{W^\star\}}{\lambda_1\{W^\star\}}$
LVRT-a(r)	0.5	1.0	0.0	4.6×10^{-10}	fail
LVRT-b(r)	0.5	0.5	0.0	6.3×10^{-11}	fail
LVRT-c(r)	0.1	0.1	0.0	5.1×10^{-10}	fail
HVRT-a(r)	1.3	1.0	-1.0	9.7×10^{-11}	fail
VUA-a(r)	0.3	1.0	-1.0	1.9×10^{-10}	fail
VUA-b(r)	0.01	1.0	-1.0	4.6×10^{-9}	fail
LVRT-a(m)	0.5	1.0	0.0	9.0×10^{-10}	fail
LVRT-b(m)	0.5	0.5	0.0	3.6×10^{-10}	fail
LVRT-c(m)	0.1	0.1	0.0	1.2×10^{-10}	fail
HVRT-a(m)	1.3	1.0	-1.0	9.5×10^{-11}	fail
VUA-a(m)	0.3	1.0	-1.0	1.8×10^{-10}	fail
VUA-b(m)	0.01	1.0	-1.0	1.6×10^{-7}	fail

TABLE II
Numerical Results of IEEE 69-Bus Test Feeder

Case	V_s	$\frac{P_i^{\max}}{S_i}$	$\frac{P_i^{\min}}{S_i}$	$\frac{\lambda_2\{X^\star\}}{\lambda_1\{X^\star\}}$	$\frac{\lambda_2\{W^\star\}}{\lambda_1\{W^\star\}}$
LVRT-a	0.5	1.0	0.0	3.6×10^{-8}	fail
LVRT-b	0.5	0.5	0.0	3.3×10^{-8}	fail
LVRT-c	0.1	0.1	0.0	2.3×10^{-8}	fail
HVRT-a	1.3	1.0	-1.0	3.0×10^{-8}	fail
VUA-a	0.3	1.0	-1.0	1.3×10^{-8}	fail
VUA-b	0.1	1.0	-1.0	3.1×10^{-7}	fail

- The symbol 'r' ('m') stands for the radial (meshed) case where the looping branches are open (closed) in the IEEE 33-bus test system. All the other three systems are radial.
- The quantities $P_i^{\max}/S_i$ and $P_i^{\min}/S_i$ represent the active power availability of IBRs; $P_i^{\min}/S_i < 0$ means that IBRs may serve as power sinks, such as energy storage.
- $\lambda_2\{\cdot\}/\lambda_1\{\cdot\}$ stands for the ratio between the two largest eigenvalues of a matrix, quantifying its closeness to rank one.

It can be observed from Tables I–IV that $\lambda_2\{X^\star\}/\lambda_1\{X^\star\}$ is of the order $O(10^{-7})$ or smaller for the c-SDP, indicating that the c-SDP is numerically exact in all test cases. Despite the equivalence of the v-SDP, when solving it, the solver runs into numerical problems and terminates with considerable constraint violations and duality gap in all the test cases. For example, the nonzero model parameters associated with the IEEE 33-bus system in LVRT-a(r) range from 0.25 to 7.8×10^6 in absolute value, with the maximum associated with $H_2^{\rm c}$; more specifically, $|2\mathrm{Re}\{Y_{21}^{\mathsf{H}} Y_{22}\}| = 7.8 \times 10^6$. Similar behavior is observed when using other SDP solvers, such as MOSEK, further supporting the conjecture made in Section IV. Moreover, the exactness of the SDP relaxation is guaranteed for both radial and meshed network topologies, demonstrating the topology-neutral nature of the proposed coDVS method.

Notably, when a very small negative-sequence voltage is set, one might intuitively expect that such a small voltage unbalance can be fully mitigated by IBRs; however, this may not be true even when the negative-sequence voltage is infinitesimal. This limitation arises from the relationship between the cardinalities of the sets $\mathcal{K}$ and $\mathcal{G}$; more specifically, it is only possible to achieve full mitigation of VU over a limited set of critical buses such that $|\mathcal{K}| \leq |\mathcal{G}|$. This is because if $|\mathcal{K}| > |\mathcal{G}|$, enforcing full mitigation of negative sequence voltage yields yields an overdetermined system of linear equations that ad-

TABLE III
NUMERICAL RESULTS OF UKGDS 95-BUS TEST FEEDER

Case	V_s	$\frac{P_i^{\max}}{S_i}$	$\frac{P_i^{\min}}{S_i}$	$\frac{\lambda_2\{X^\star\}}{\lambda_1\{X^\star\}}$	$\frac{\lambda_2\{W^\star\}}{\lambda_1\{W^\star\}}$
LVRT-a	0.5	1.0	0.0	1.9×10^{-10}	fail
LVRT-b	0.5	0.5	0.0	1.2×10^{-10}	fail
LVRT-c	0.1	0.1	0.0	1.0×10^{-8}	fail
HVRT-a	1.3	1.0	-1.0	1.7×10^{-11}	fail
VUA-a	0.3	1.0	-1.0	3.0×10^{-11}	fail
VUA-b	0.1	1.0	-1.0	3.9×10^{-7}	fail

TABLE IV
NUMERICAL RESULTS OF 3146-BUS TEST FEEDER

Case	V_s	$\frac{P_i^{\max}}{S_i}$	$\frac{P_i^{\min}}{S_i}$	$\frac{\lambda_2\{X^\star\}}{\lambda_1\{X^\star\}}$	$\frac{\lambda_2\{W^\star\}}{\lambda_1\{W^\star\}}$
LVRT-a	0.5	1.0	0.0	1.1×10^{-10}	fail
LVRT-b	0.5	0.5	0.0	1.5×10^{-10}	fail
LVRT-c	0.1	0.1	0.0	1.8×10^{-9}	fail
HVRT-a	1.3	1.0	-1.0	5.4×10^{-11}	fail
VUA-a	0.3	1.0	-1.0	1.3×10^{-10}	fail
VUA-b	0.1	1.0	-1.0	3.5×10^{-11}	fail

TABLE V
NUMERICAL RESULTS WITH NON-DISPATCHABLE IBRS

Case	Complex power injections $S_i = P_i + \mathrm{j}Q_i$	$\frac{\lambda_2\{X^\star\}}{\lambda_1\{X^\star\}}$
1	$1.00+\mathrm{j}0.83, 1.00+\mathrm{j}1.01, 1.00+\mathrm{j}0.87$ $\mathbf{Bus\ 25,33:\ 1.00+j0.00, 1.00+j0.00}$	2.44×10^{-9}
2	$1.00+\mathrm{j}0.71, 1.00+\mathrm{j}0.91, 0.96+\mathrm{j}0.81$ $\mathbf{Bus\ 25,33:\ 0.80+j0.30, 0.80+j0.30}$	5.51×10^{-9}

TABLE VI
EXECUTION TIMES FOR OPTIMIZATION

Test System	Modeling Time [s] (YALMIP)	Solver Time [s]	
		MOSEK	SeDuMi
33-bus (5 IBRs)	0.0055	0.0025	0.0173
69-bus (7 IBRs)	0.0136	0.0043	0.0249
95-bus (8 IBRs)	0.0161	0.0059	0.0060
3146-bus (20 IBRs)	0.0119	0.0381	0.3876
3146-bus (50 IBRs)	0.0243	1.1077	32.653
3146-bus (100 IBRs)	0.0386	23.544	N/A

mits no exact solution. As exemplified by Case VUA-b(r), full mitigation is theoretically infeasible regardless of the overcurrent capacity provided, where $|\mathcal{K}| = |\mathcal{N}| > |\mathcal{G}|$.

B. Incorporation of Non-dispatchable IBRs

To verify the effectiveness of the proposed framework in the presence of non-dispatchable IBRs, we conducted test cases on the IEEE 33-bus system. Specifically, the IBRs at Bus 25 and Bus 33 are assumed to be non-dispatchable, maintaining their pre-fault power outputs throughout the disturbance.

- Case 1: $V_s = 0.85$ pu, $P_{25}^{\mathrm{ref}} = P_{33}^{\mathrm{ref}} = 1$ pu and $Q_{25}^{\mathrm{ref}} = Q_{33}^{\mathrm{ref}} = 0$ pu.
- Case 2: $V_s = 0.80$ pu, $P_{25}^{\mathrm{ref}} = P_{33}^{\mathrm{ref}} = 0.8$ pu and $Q_{25}^{\mathrm{ref}} = Q_{33}^{\mathrm{ref}} = 0.3$ pu.

The numerical results are summarized in Table V. It shows that even accounting for the impact of non-dispatchable IBRs, the SDP relaxation remains exact. Furthermore, the power injections of the two non-dispatchable IBRs (indicated in bold) strictly track their references. These results confirm that the coDVS framework can naturally accommodate heterogeneously controlled IBRs across the network.

C. Execution Times for Optimization

The execution times for the optimization (LVRT-a as an example) are reported in Table VI. All simulations are conducted on a PC with an Intel Core i9 processor and 64 GB RAM, using SeDuMi and MOSEK [38] (interfaced by YALMIP) as the SDP solvers. The results indicate that, for a moderate number of IBRs, off-the-shelf SDP solvers (e.g., MOSEK) can obtain solutions within $2 \sim 3$ fundamental cycles (< 50 ms), which meets the stringent DVS response time requirements specified in modern grid codes and interconnection standards [29]. However, as the problem size increases—primarily driven by the number of integrated IBRs—the solver time increases substantially, rendering centralized implementations incompatible with fast real-time DVS control. Continued advancements in hardware and algorithms may further reduce solver latency [39], [40]. Moreover, developing a decentralized implementation of the proposed framework is a promising solution to enhance its scalability in large-scale systems, which will be left for our future work.

VII. DYNAMIC SIMULATION

To thoroughly validate the optimal coDVS strategy, we further perform dynamic simulations on the IEEE 33-bus system in MATLAB/Simulink environment and compare it with the widely-used droop-based control strategy ('droop control' for short). The droop control is selected as the baseline for comparison because it represents the prevailing industrial benchmark strictly mandated by the latest grid codes [41], [42] and widely adopted in recent practices [6], [8]. The coDVS strategy is implemented by solving the c-SDP due to better numerical stability. Fig. 1 in Section II illustrates the configuration of the IEEE 33-bus test feeder. The PV panel is composed of four 250 kW arrays connected in parallel. Bus 18 is selected as a representative node to present the results in most cases.

A. Test of LVRT

For implementation, the optimal current injections $I_i^\star, i \in \mathcal{G}$ obtained from the c-SDP need to be converted into dq-frame current references corresponding to the local voltages by

$$I_i^{\mathrm{d}} = \mathrm{Re}\left\{\frac{I_i^\star (V_i^\star)^{\mathsf{H}}}{|V_i^\star|}\right\}, \quad I_i^{\mathrm{q}} = \mathrm{Im}\left\{\frac{I_i^\star (V_i^\star)^{\mathsf{H}}}{|V_i^\star|}\right\} \tag{15}$$

where $V_i^\star = \mathbf{e}_i^{\mathsf{T}} Z \mathbf{i}^\star$.

In Case A, a voltage sag with $V_s = 0.3$ pu strikes at $t = 0.3$ s, with the power availability of IBRs being 1.0 pu. The LVRT is triggered when the substation positive-sequence voltage is less than 0.85 pu [42]. With the proposed coDVS strategy, PV inverters inject the optimized active and reactive currents for DVS while respecting their current and power constraints. The droop control prioritizes reactive current injections; thus, the active current may be reduced to nearly zero due to the current limit. It can be seen in Fig. 2 that the proposed coDVS shows noticeable advantage over the droop control in terms of DVS

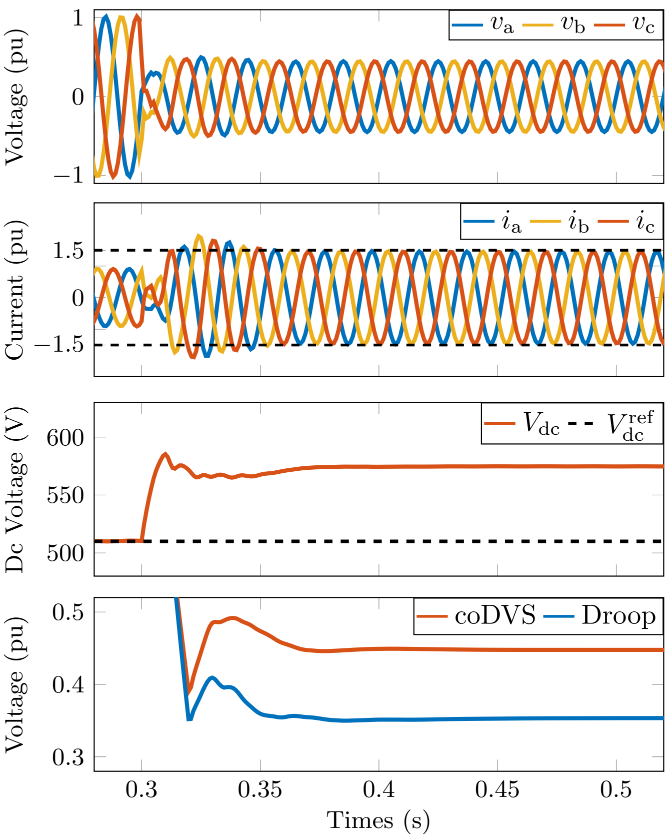

Fig. 2. Simulation results associated with Bus 18 in Case A. From top to bottom: three-phase voltages, three-phase inverter current injections, dc voltage of inverter, and positive-sequence voltage with different control strategies.

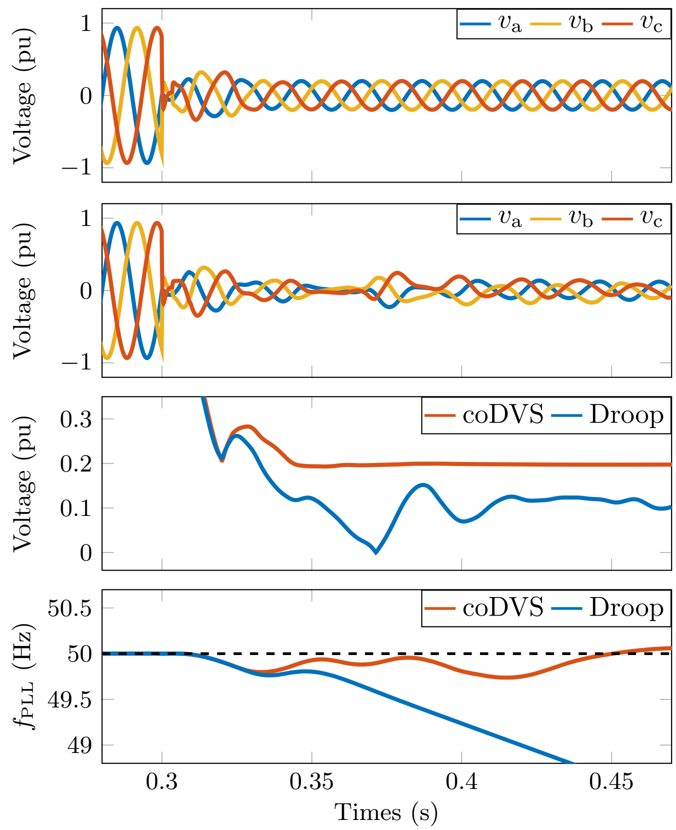

Fig. 3. Simulation results associated with Bus 18 in Case B. From top to bottom: three-phase voltages with coDVS, three-phase voltages with droop control, positive-sequence voltage and PLL frequency with different control strategies.

capability (0.45 pu with coDVS vs. 0.35 pu with the droop control). Due to the self-protection nature of single-stage PV, the dc voltage is boosted to a new equilibrium with a lower power production corresponding to the optimal DVS behavior.

In Case B, a severe voltage sag of $V_s = 0.1$ pu occurs at $t = 0.3$ s, with the power availability of IBRs being 0.1 pu. As shown in Fig. 3, the droop control results in loss of synchronism (LoS), which can be reflected by the continuous excursion of the phase locked-loop (PLL) frequency. This instability arises from an aggressive reactive current injection that disrupts system equilibrium, consistent with findings from the single IBR scenarios reported in [10]. In contrast, the coDVS approach can still keep the synchronism between the PV systems and the distribution network, while substantially boosting network voltages. Notably, as observed in Fig. 3, the PLL frequency under the coDVS remains within $49.7 \sim 50.1$ Hz, satisfying grid-connected operation requirements specified in grid codes (see [42] for example). This may help prevent trip-offs of PV systems under severe voltage dips, highlighting the need for more effective coordination.

B. Test of HVRT

We also conduct dynamic simulations for HVRT scenarios. In order to provide effective sequence voltage attenuation, the IBRs shall possess the capability of absorbing a certain amount of power. In this context, a small energy storage is additionally introduced with a power rating of 30% in parallel with the PV systems at the dc side. Once the HVRT is triggered, the PV panels opt out, while the IBRs can absorb power through the dedicated dc-side energy storage. In Case C, a positive-sequence voltage swell strikes at $t = 0.3$ s with $V_s = 1.3$ pu. The HVRT is triggered when the positive-sequence voltage at the substation is higher than 1.1 pu [42]. As shown in Fig. 4, the droop control restores the positive-sequence voltage at Bus 18 to 1.17 pu. In contrast, the proposed coDVS mitigates the swell further, achieving a much lower voltage of 1.07 pu.

C. Tests of VUA

The same system configuration used for the HVRT is applied in the VUA scenarios. In Case D, an unbalanced voltage sag is simulated, with the positive- and negative-sequence voltages of $0.5\angle 0°$ pu and $0.3\angle 50°$ pu, respectively. The primary goal of coDVS in the VUA is to suppress the negative-sequence voltage. It is triggered when the negative-sequence voltage at the substation is larger than 0.05 pu. The decoupled positive- and negative-sequence control is adopted [43]. Since the PLL cannot precisely track the negative-sequence voltage when it is largely attenuated, the current references obtained by (15) under the negative-sequence dq frame are mapped to the positive-sequence dq frame for implementation. [3]

[3] Consequently, the phase angle difference between the two reference frames is determined by commanding the IBR to inject zero currents during the first three cycles after VUA activation. See [11] for more details.

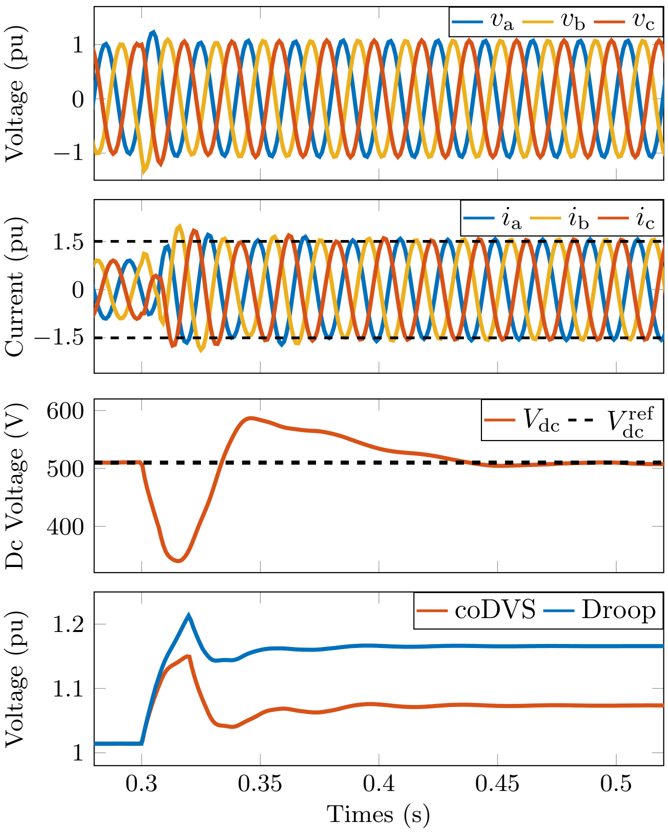

Fig. 4. Simulation results associated with Bus 18 in Case C. From top to bottom: three-phase voltages, three-phase inverter current injections, dc voltage of inverter, and positive-sequence voltage with different control strategies.

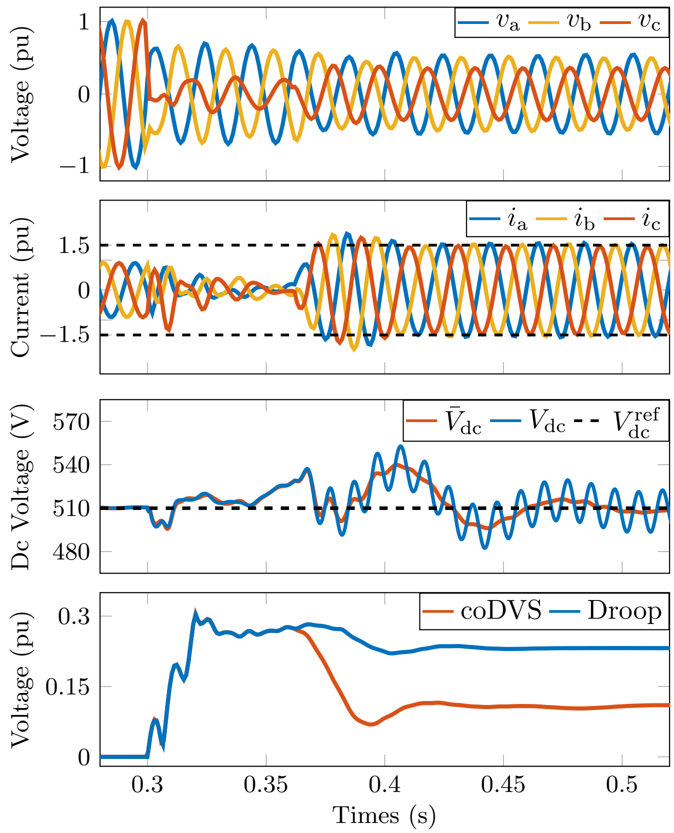

Fig. 5. Simulation results associated with Bus 18 in Case D. From top to bottom: three-phase voltages, three-phase inverter current injections, inverter dc voltage ($\bar{V}_{dc}$ denotes the filtered value), and negative-sequence voltage with different control strategies.

The simulation results are depicted in Fig. 5. It can be seen that the negative-sequence voltage at Bus 18 is reduced to 0.11 pu under the coDVS, compared to 0.23 pu under the droop control. Using the coDVS, the (filtered) dc voltage of the IBR converges to the pre-fault value asymptotically, indicating a power re-balance at the dc side thanks to the power absorption of energy storage. This demonstrates the ability of coDVS in mitigating voltage unbalance.

In Case E, a minor voltage unbalance is characterized by 0.01 pu negative-sequence voltage and 1.0 pu positive-sequence voltage at the slack bus. At $t = 0.3$ s, the coDVS is triggered to fully mitigate VU at the five IBR buses.[4] As shown in Fig. 6, the negative-sequence voltages at the five IBR buses are fully mitigated, with none of the IBRs reaching its current limit. This verifies the findings discussed in Section VI-A. By contrast, the droop control fails to fully mitigate the negative-sequence voltages, and instead a pronounced oscillation is observed, likely due to the difficulty in accurately tracking the phase angle of minor negative-sequence voltages.

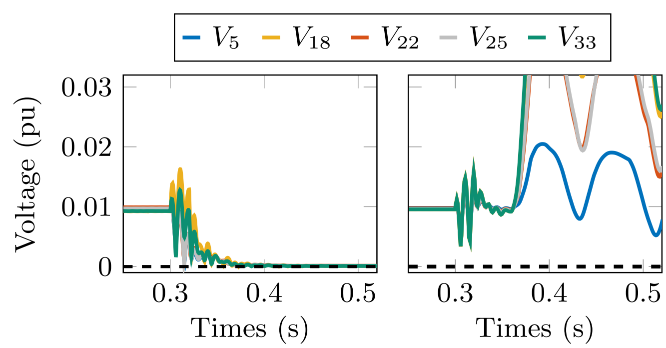

Fig. 6. Simulation results associated with IBR buses in Case E ($\mathcal{K} = \mathcal{G} = \{5, 18, 22, 25, 33\}$). Left: negative-sequence voltages with coDVS; right: negative-sequence voltages with droop control.

VIII. Conclusion

This paper focuses on the multi-IBR coordinated dynamic voltage support in distribution networks under various conditions (voltage sag, swell, and unbalance). The problem is formulated as a nonconvex QCQP, and a convex (SDP) relaxation approach is proposed. The main findings are summarized as follows:

1) The SDP relaxation is generally exact for the coDVS problems, as validated on four test feeders. This allows the retrieval of globally optimal solutions to the original nonconvex programs via spectral decomposition.
2) A theoretical equivalence exists between the current-based and voltage-based formulations, which holds true even under the SDP relaxation. In particular, the exactness of either the c-SDP or v-SDP formulation necessarily

[4]Here, it is assumed that the magnitude and phase angle of the negative-sequence voltage at the slack bus can be accurately measured, and the network model is precise. Based on this, the phase angle differences can be calculated, and the optimal current references are supplied to the inverter control loops in a feedforward manner.

implies the exactness of the other.

3) Voltage-based formulations are prone to numerical issues due to their ill-conditioned nature, primarily caused by the inverter current constraints, and are therefore not recommended for practical use.
4) A full mitigation of voltage unbalance can be achieved in theory only if the number of IBRs is equal to or larger than that of the critical buses to be optimized.
5) It is demonstrated that the coDVS provides superior voltage support compared to the conventional droop control, while maintaining the synchronization stability of IBRs under severe voltage sags.

This work not only delivers the globally optimal solution to the coordinated dynamic voltage support and its associated optimal control, but also establishes a benchmark for evaluating alternative control strategies. Although the analysis throughout this work is framed in the context of distribution networks, the methods and results are broadly applicable to other systems with similar characteristics—such as microgrids, wind or solar farm collector systems, and regional transmission networks—provided that voltage disturbances originate externally to the network under consideration.

While the exactness of SDP relaxation has been numerically verified across various test cases, it still remains mysterious whether this generally holds in practice. Furthermore, the centralized framework may face scalability challenges in large-scale systems, primarily due to computational bottlenecks and the substantial overhead associated with dedicated infrastructure, thereby necessitating the exploration of a decentralized implementation. Finally, accurately capturing the dynamics of IBRs within the optimization is essential for ensuring their robust performance and secure operation under large disturbances, and thus deserves further investigation. These critical questions are left for future study.

APPENDIX A PROOF OF LEMMA 1

Proof: We first show that the mapping f is well-defined, and then prove that it is bijective.

Well-defined: The well-definedness of f means that for any $X \in \mathbb{X}$, there exists a unique $W \in \mathbb{W}$ such that $W = f(X)$.

For every $X \in \mathbb{X}$, let $W = f(X) = ZXZ^{\mathsf{H}}$.

The fact that W is uniquely determined trivially holds true given the matrix operations defined in f. Thus, we only need to show $W \in \mathbb{W}$.

a) Since $X \in \mathbb{H}^n$, $W^{\mathsf{H}} = (ZXZ^{\mathsf{H}})^{\mathsf{H}} = ZX^{\mathsf{H}}Z^{\mathsf{H}} = ZXZ^{\mathsf{H}} = W$. So, we have $W \in \mathbb{H}^n$.

b) Then, it follows from the *cyclic property* of the trace that

$$\begin{aligned}
\mathrm{Tr}\{H_i^{\mathrm{c}}W\} &= \mathrm{Tr}\{Y^{\mathsf{H}}\mathbf{e}_i\mathbf{e}_i^{\mathsf{T}}YZXZ^{\mathsf{H}}\} \\
&= \mathrm{Tr}\{(YZ)^{\mathsf{H}}\mathbf{e}_i\mathbf{e}_i^{\mathsf{T}}YZX\} \\
&= \mathrm{Tr}\{M_i^{\mathrm{c}}X\} \leq (I_i^{\max})^2 \\
\mathrm{Tr}\{H_i^{\mathrm{p}}W\} &= \frac{1}{2}\mathrm{Tr}\{(Y^{\mathsf{H}}\mathbf{e}_i\mathbf{e}_i^{\mathsf{T}} + \mathbf{e}_i\mathbf{e}_i^{\mathsf{T}}Y)ZXZ^{\mathsf{H}}\} \\
&= \frac{1}{2}\mathrm{Tr}\{(YZ)^{\mathsf{H}}\mathbf{e}_i\mathbf{e}_i^{\mathsf{T}}ZX + Z^{\mathsf{H}}\mathbf{e}_i\mathbf{e}_i^{\mathsf{T}}YZX\} \\
&= \frac{1}{2}\mathrm{Tr}\{\left(\mathbf{e}_i\mathbf{e}_i^{\mathsf{T}}Z + Z^{\mathsf{H}}\mathbf{e}_i\mathbf{e}_i^{\mathsf{T}}\right)X\} \\
&= \mathrm{Tr}\{M_i^{\mathrm{p}}X\} \in [P_i^{\min}, P_i^{\max}]
\end{aligned}$$

$$\begin{aligned}
\mathrm{Tr}\{H_s^{\mathrm{v}}W\} &= \mathrm{Tr}\{\mathbf{e}_1\mathbf{e}_1^{\mathsf{T}}ZXZ^{\mathsf{H}}\} \\
&= \mathrm{Tr}\{Z^{\mathsf{H}}\mathbf{e}_1\mathbf{e}_1^{\mathsf{T}}ZX\} \\
&= \mathrm{Tr}\{M_s^{\mathrm{v}}X\} = V_s^2
\end{aligned}$$

c) For any nonzero vector $\xi \in \mathbb{C}^n$, it follows that

$$\xi^{\mathsf{H}}W\xi = (Z^{\mathsf{H}}\xi)^{\mathsf{H}}X(Z^{\mathsf{H}}\xi) \succeq 0.$$

So, we have $W \in \mathbb{W}$. This completes the proof of well-definedness.

Now, we prove that f is bijective.

Surjective: For any $W \in \mathbb{W}$, let $X = YWY^{\mathsf{H}}$. Then, it follows immediately that

$$f(X) = ZXZ^{\mathsf{H}} = ZYWY^{\mathsf{H}}Z^{\mathsf{H}} = W.$$

Next, we need to show that $X \in \mathbb{X}$.

a) Since $W \in \mathbb{H}^n$, $X^{\mathsf{H}} = (YWY^{\mathsf{H}})^{\mathsf{H}} = X \in \mathbb{H}^n$.

b) Then, it follows from the *cyclic property* of the trace that

$$\begin{aligned}
\mathrm{Tr}\{M_i^{\mathrm{c}}X\} &= \mathrm{Tr}\{\mathbf{e}_i\mathbf{e}_i^{\mathsf{T}}YWY^{\mathsf{H}}\} \\
&= \mathrm{Tr}\{Y^{\mathsf{H}}\mathbf{e}_i\mathbf{e}_i^{\mathsf{T}}YW\} \\
&= \mathrm{Tr}\{H_i^{\mathrm{c}}W\} \leq (I_i^{\max})^2 \\
\mathrm{Tr}\{M_i^{\mathrm{p}}X\} &= \frac{1}{2}\mathrm{Tr}\{(Z^{\mathsf{H}}\mathbf{e}_i\mathbf{e}_i^{\mathsf{T}} + \mathbf{e}_i\mathbf{e}_i^{\mathsf{T}}Z)YWY^{\mathsf{H}}\} \\
&= \frac{1}{2}\mathrm{Tr}\{(ZY)^{\mathsf{H}}\mathbf{e}_i\mathbf{e}_i^{\mathsf{T}}YW + Y^{\mathsf{H}}\mathbf{e}_i\mathbf{e}_i^{\mathsf{T}}ZYW\} \\
&= \frac{1}{2}\mathrm{Tr}\left\{\left(\mathbf{e}_i\mathbf{e}_i^{\mathsf{T}}Y + Y^{\mathsf{H}}\mathbf{e}_i\mathbf{e}_i^{\mathsf{T}}\right)W\right\} \\
&= \mathrm{Tr}\{H_i^{\mathrm{p}}W\} \in [P_i^{\min}, P_i^{\max}] \\
\mathrm{Tr}\{M_s^{\mathrm{v}}X\} &= \mathrm{Tr}\{Z^{\mathsf{H}}\mathbf{e}_1\mathbf{e}_1^{\mathsf{T}}ZYWY^{\mathsf{H}}\} \\
&= \mathrm{Tr}\{(ZY)^{\mathsf{H}}\mathbf{e}_1\mathbf{e}_1^{\mathsf{T}}ZYW\} \\
&= \mathrm{Tr}\{\mathbf{e}_1\mathbf{e}_1^{\mathsf{T}}W\} \\
&= \mathrm{Tr}\{H_s^{\mathrm{v}}W\} = V_s^2
\end{aligned}$$

c) For any nonzero vector $\xi \in \mathbb{C}^n$, it follows that

$$\xi^{\mathsf{H}}X\xi = (Y^{\mathsf{H}}\xi)^{\mathsf{H}}W(Y^{\mathsf{H}}\xi) \succeq 0.$$

So, $X \in \mathbb{X}$ is a *preimage* of W.

Injective: Assume by contradiction that there exist some $X_1 \neq X_2 \in \mathbb{X}$ such that $f(X_1) = f(X_2)$. Then, we have

$$\begin{aligned}
& ZX_1Z^{\mathsf{H}} = ZX_2Z^{\mathsf{H}} \\
\Rightarrow\ & YZX_1Z^{\mathsf{H}}Y^{\mathsf{H}} = YZX_2Z^{\mathsf{H}}Y^{\mathsf{H}} \\
\Rightarrow\ & X_1 = X_2
\end{aligned}$$

which gives a contradiction. So, the preimage must be unique for any $W \in \mathbb{W}$. This completes the proof that f is bijective.

Further, it is straightforward to verify that $f \circ g$ and $g \circ f$ are identity mappings. This completes the proof of Lemma 1. ■

REFERENCES

[1] A. Cabrera-Tobar, E. Bullich-Massagué, M. Aragüés-Peñalba, and O. Gomis-Bellmunt, "Review of advanced grid requirements for the integration of large scale photovoltaic power plants in the transmission system," *Renew. Sustain. Energy Rev.*, vol. 62, pp. 971–987, 2016.

[2] K. Zeb, S. U. Islam, I. Khan, W. Uddin, M. Ishfaq, T. D. C. Busarello *et al.*, "Faults and fault ride through strategies for grid-connected photovoltaic system: A comprehensive review," *Renew. Sustain. Energy Rev.*, vol. 158, 2022, Art. no. 112125.

[3] *IEEE Standard for Interconnection and Interoperability of Distributed Energy Resources With Associated Electric Power Systems Interfaces*, IEEE Std. 1547-2018, 2018.

[4] T. Neumann, T. Wijnhoven, G. Deconinck, and I. Erlich, “Enhanced dynamic voltage control of type 4 wind turbines during unbalanced grid faults,” *IEEE Trans. Energy Convers.*, vol. 30, no. 4, pp. 1650–1659, 2015.

[5] M. M. Shabestary and Y. A.-R. I. Mohamed, “Asymmetrical ride-through and grid support in converter-interfaced DG units under unbalanced conditions,” *IEEE Trans. Ind. Electron.*, vol. 66, no. 2, pp. 1130–1141, 2019.

[6] X. Lyu, Y. Jia, T. Liu, and Y. He, “Concurrent optimal re/active power control for wind farms under low-voltage-ride-through operation,” *IEEE Trans. Power Syst.*, vol. 35, no. 6, pp. 4956–4959, 2020.

[7] M. Graungaard Taul, X. Wang, P. Davari, and F. Blaabjerg, “Current reference generation based on next-generation grid code requirements of grid-tied converters during asymmetrical faults,” *IEEE J. Emerg. Sel. Topics Power Electron.*, vol. 8, no. 4, pp. 3784–3797, 2020.

[8] A. Azizi, A. Banaiemoqadam, A. Hooshyar, and M. Patel, “A blind spot in the LVRT current requirements of modern grid codes for inverter-based resources,” *IEEE Trans. Power Del.*, vol. 38, no. 1, pp. 319–334, 2023.

[9] A. Camacho, M. Castilla, J. Miret, L. G. de Vicuña, and R. Guzman, “Positive and negative sequence control strategies to maximize the voltage support in resistive–inductive grids during grid faults,” *IEEE Trans. Power Electron.*, vol. 33, no. 6, pp. 5362–5373, 2018.

[10] Y. Guo, B. C. Pal, R. A. Jabr, and H. Geng, “Global optimality of inverter dynamic voltage support,” *IEEE Trans. Power Syst.*, vol. 37, no. 5, pp. 3947–3957, 2022.

[11] Y. Guo, B. C. Pal, and R. A. Jabr, “On the optimality of voltage unbalance attenuation by inverters,” *IEEE Trans. Sustain. Energy*, vol. 13, no. 3, pp. 1492–1506, 2022.

[12] C. Zhao, D. Sun, X. Duan, and H. Nian, “Current reference optimization for inverter-based resources to mitigate grid voltage unbalance factor,” *IEEE Trans. Power Syst.*, vol. 39, no. 4, pp. 6103–6106, 2024.

[13] Y. Lin, J. H. Eto, B. B. Johnson, J. D. Flicker, R. H. Lasseter, H. N. Villegas Pico *et al.*, “Research roadmap on grid-forming inverters,” Nat. Renew. Energy Lab. (NREL), Golden, CO, USA, Tech. Rep., 2020.

[14] M. M. Shabestary and Y. A.-R. I. Mohamed, “Autonomous coordinated control scheme for cooperative asymmetric low-voltage ride-through and grid support in active distribution networks with multiple DG units,” *IEEE Trans. Smart Grid*, vol. 11, no. 3, pp. 2125–2139, 2020.

[15] X. Liu, X. Chen, C. Li, M. Shahidehpour, K. Sun, Y. Cao *et al.*, “Multi-stage voltage support optimization for microgrids with multiple distributed generation units,” *IEEE Trans. Smart Grid*, vol. 12, no. 1, pp. 141–156, 2021.

[16] Á. Borrell, M. Velasco, J. Miret, A. Camacho, P. Martí, and M. Castilla, “Collaborative voltage unbalance elimination in grid-connected AC microgrids with grid-feeding inverters,” *IEEE Trans. Power Electron.*, vol. 36, no. 6, pp. 7189–7201, 2021.

[17] M. M. Shabestary and Y. A.-R. I. Mohamed, “Maximum asymmetrical support in parallel-operated grid-interactive smart inverters,” *IEEE Trans. Sustain. Energy*, vol. 13, no. 1, pp. 14–30, 2022.

[18] R. Qiu and C. Liu, “Adaptive dynamic voltage support scheme for multiple grid-forming converters in distributed networks,” *IEEE Trans. Energy Convers.*, vol. 40, no. 3, pp. 2624–2641, 2025.

[19] M. Cintuglu and D. Ishchenko, “Multiagent-based dynamic voltage support of power converters during fault ride-through,” *IEEE J. Emerg. Sel. Topics Ind. Electron.*, vol. 3, no. 3, pp. 549–558, 2022.

[20] G. Zhang, X. Wang, and F. Gao, “Sequential dynamics in photovoltaic power station under low voltage ride through,” *IEEE Trans. Energy Convers.*, vol. 39, no. 2, pp. 1024–1033, 2024.

[21] J. Wei, Y. Cao, Q. Wu, C. Li, S. Huang, B. Zhou, and D. Xu, “Coordinated droop control and adaptive model predictive control for enhancing HVRT and post-event recovery of large-scale wind farm,” *IEEE Trans. Sustain. Energy*, vol. 12, no. 3, pp. 1549–1560, 2021.

[22] J. Wei, L. Wei, S. Huang, B. Wang, G. Huang, F. Shen, and P. Wang, “Optimal coordinated post-event voltage control with energy storage boundary analysis for large-scale wind farms,” *IEEE Trans. Power Syst.*, vol. 40, no. 4, pp. 3374–3387, 2025.

[23] Z. Lv, B. Wang, Q. Guo, and H. Sun, “Optimal grid-support strategy with inverter-interfaced distributed generators for short-term voltage stability improvement,” *IEEE Trans. Sustain. Energy*, vol. 15, no. 1, pp. 499–512, 2024.

[24] P. S. Pavankumar Y and S. Debnath, “Multi-objective Pareto optimal unbalance voltage compensation in the microgrid,” *Electr. Power Syst. Res.*, vol. 217, 2023, Art. no. 109104.

[25] D. K. Molzahn, F. Dörfler, H. Sandberg, S. H. Low, S. Chakrabarti, R. Baldick *et al.*, “A survey of distributed optimization and control algorithms for electric power systems,” *IEEE Trans. Smart Grid*, vol. 8, no. 6, pp. 2941–2962, 2017.

[26] R. S. Sutton, A. G. Barto *et al.*, *Reinforcement learning: An introduction*. MIT press Cambridge, 1998, vol. 1, no. 1.

[27] S. Karagiannopoulos, P. Aristidou, and G. Hug, “Data-driven local control design for active distribution grids using off-line optimal power flow and machine learning techniques,” *IEEE Trans. Smart Grid*, vol. 10, no. 6, pp. 6461–6471, 2019.

[28] D. Turizo and D. K. Molzahn, “Invertibility conditions for the admittance matrices of balanced power systems,” *IEEE Trans. Power Syst.*, vol. 38, no. 4, pp. 3841–3853, 2023.

[29] *IEEE Standard for Interconnection and Interoperability of Inverter-Based Resources (IBRs) Interconnecting with Associated Transmission Electric Power Systems*, IEEE Std. 2800-2022, 2022.

[30] R. Teodorescu, M. Liserre, and P. Rodriguez, *Grid Converters for Photovoltaic and Wind Power Systems*. John Wiley & Sons, 2011.

[31] D. Bertsekas, *Convex Optimization Theory*. Athena Scientific, 2009.

[32] M. E. Baran and F. F. Wu, “Network reconfiguration in distribution systems for loss reduction and load balancing,” *IEEE Trans. Power Del.*, vol. 4, no. 2, pp. 1401–1407, 1989.

[33] M. Baran and F. Wu, “Optimal capacitor placement on radial distribution systems,” *IEEE Trans. Power Del.*, vol. 4, no. 1, pp. 725–734, 1989.

[34] R. Singh, B. C. Pal, and R. A. Jabr, “Statistical representation of distribution system loads using Gaussian mixture model,” *IEEE Trans. Power Syst.*, vol. 25, no. 1, pp. 29–37, 2010.

[35] R. A. Jabr, “Robust volt/var control with photovoltaics,” *IEEE Trans. Power Syst.*, vol. 34, no. 3, pp. 2401–2408, 2019.

[36] J. F. Sturm, “Using SeDuMi 1.02, a MATLAB toolbox for optimization over symmetric cones,” *Optim. Methods Softw.*, vol. 11, no. 1-4, pp. 625–653, 1999.

[37] J. Löfberg, “YALMIP: A toolbox for modeling and optimization in MATLAB,” in *Proc. IEEE CACSD Conf.*, Taipei, Taiwan, 2004.

[38] M. ApS, “Mosek optimization toolbox for MATLAB,” *User’s Guide and Reference Manual, Version 11.1.11*, Apr. 2026.

[39] J. L. Hennessy and D. A. Patterson, “A new golden age for computer architecture,” *Commun. ACM*, vol. 62, no. 2, pp. 48–60, Jan. 2019. [Online]. Available: https://doi.org/10.1145/3282307

[40] A. Majumdar, G. Hall, and A. A. Ahmadi, “Recent scalability improvements for semidefinite programming with applications in machine learning, control, and robotics,” *Annu. Rev. Control Robot. Auton. Syst.*, vol. 3, no. 1, pp. 331–360, 2020.

[41] *Summary of the draft, VDE-AR-N 4120:2017-05*, VDE Std., May 2017.

[42] *Technical Requirements for Connecting Photovoltaic Power System to Distribution Network*, Std. GB/T 29 319-2024, 2024.

[43] H.-S. Song and K. Nam, “Dual current control scheme for PWM converter under unbalanced input voltage conditions,” *IEEE Trans. Ind. Electron.*, vol. 46, no. 5, pp. 953–959, 1999.